available at www.sciencedirect.com

ScienceDirect

journal homepage: http://www.rpor.eu/


Original article

# Differential dose contributions on total dose distribution of $^{125}$I brachytherapy source

B. Camgöz[a,*], G. Yeğin[b], M.N. Kumru[a]

[a] Ege University Institute of Nuclear Sciences, Izmir, Turkey
[b] Celal Bayar Univesity Science Faculty-Physics Depatment, Manisa, Turkey

ARTICLE INFO

*Article history:*
Received 1 February 2010
Received in revised form
29 March 2010
Accepted 23 April 2010

*Keywords:*
Monte Carlo
Brachytherapy
Radiation dose

ABSTRACT

This work provides an improvement of the approach using Monte Carlo simulation for the Amersham Model 6711 $^{125}$I brachytherapy seed source, which is well known by many theoretical and experimental studies. The source which has simple geometry was researched with respect to criteria of AAPM Tg-43 Report. The approach offered by this study involves determination of differential dose contributions that come from virtual partitions of a massive radioactive element of the studied source to a total dose at analytical calculation point. Some brachytherapy seeds contain multi-radioactive elements so the dose at any point is a total of separate doses from each element. It is momentous to know well the angular and radial dose distributions around the source that is located in cancerous tissue for clinical treatments. Interior geometry of a source is effective on dose characteristics of a distribution. Dose information of inner geometrical structure of a brachytherapy source cannot be acquired by experimental methods because of limits of physical material and geometry in the healthy tissue, so Monte Carlo simulation is a required approach of the study. EGSnrc Monte Carlo simulation software was used. In the design of a simulation, the radioactive source was divided into 10 rings, partitioned but not separate from each other. All differential sources were simulated for dose calculation, and the shape of dose distribution was determined comparatively distribution of a single-complete source. In this work anisotropy function was examined also mathematically.



## 1. Introduction

In general definition, brachytherapy is a placement of radioactive sources into cancerous tissue volume at single or multiple locations. It (sometime it is mentioned as Curie therapy)[1] uses radiation of low energy that is taken into a capsule (this system is named seed) in cancer treatment.

While low-energy, photon-emitting brachytherapy sources have been used to treat cancers involving a variety of anatomical sites, including eye plaque therapy for choroidal melanoma and permanent lung implants,[2] their most frequent indication today is for the treatment of prostate cancer.[3] Prostate cancer is the most frequent type of cancer in men in the United States with approximately 180,000 new incident cases per year and an annual death rate of about 37,000.[4] While approxi-

* *Corresponding author*. Tel.: +90 2323886466.
E-mail address: berkay.camgoz@ege.edu.tr (B. Camgöz).
1507-1367/$ – see front matter © 2010 Greater Poland Cancer Centre, Poland. Published by Elsevier Urban & Partner Sp. z.o.o. All rights reserved.
doi:10.1016/j.rpor.2010.04.003

mately 60% of new cases are confined to the organ at time of diagnosis, only about 2.2% of these new cases were treated with brachytherapy in 1995. Since that time, the percentage has increased to about 30% of all eligible patients receiving implants in current practice.[5]

The aim is to apply radiation with optimum dose on cancer tissues with minimum damage to healthy ones. In clinical treatments, scientific data are taken as criteria in the use of brachytherapy sources and devices. Especially simulation studies are momentous before treatment planning as pre-examination.

Knowledge of dose distribution around radioactive sources employed in brachytherapy implants is necessary in order to provide a more solid basis when developing a clinical strategy. The AAPM TG-43 Report recommends dosimetry protocol based on measured or measurable quantities and decouples number of interrelated quantities.[6] The protocol allows two-dimensional dose calculations around cylindrically symmetric sources.[7]

Source geometry and internal construction are highly manufacturer specific. Source models vary from one another with regard to weld thickness and type, radioactivity carrier construction, presence of radio-opaque material with sharp or rounded edges, presence of silver (which produces characteristic X-rays that modify the photon spectrum), and capsule wall thickness. All of these properties can affect the dosimetric characteristics of the source.[5] Based on the results of Williamson,[8] purely Monte Carlo estimates of the transverse-axis dose-rate per unit air-kerma strength typically have uncertainties of 2–3% at 1 cm and 3–5% at 5 cm, depending on the type and magnitude of internal seed geometric uncertainties. Since relatively little has been published on estimation of systematic uncertainties of Monte Carlo-based dose estimation.[5]

In this work an approach was examined to lead to determining internal geometry effects on dose distribution. Along radioactive source axis in bachytherapy seed, radio-opaque marker which is coated by radioactive material ($^{125}$I) and active element have cylindrical geometry basically. According to the approach, the cylinder was cut into 10 partitions in Monte Carlo simulation by geometry design routine of the software. EGSnrc–dosrznrc was used for simulation of dose calculation in water phantom. There can be found several softwares for Monte Carlo simulation. Apart from EGSnrc Code, MCNP4 Code is commonly used for brachytherapy studies.[9]

In view of its suitable radiation characteristics, such as ~27.4–35 keV X and gamma radiations, reasonably long half-life of ~60 days, and ease of production in medium flux nuclear reactors, $^{125}$I is considered to be one of the best isotopes among the available options for use in both eye and prostate brachytherapy. $^{125}$I seed sources are also being tried for the treatment of various tumor sites, because their low-energy photon emissions cause a rapid decrease in dose with increasing distance and thereby minimize the dose to adjacent vital organs.[10,11]

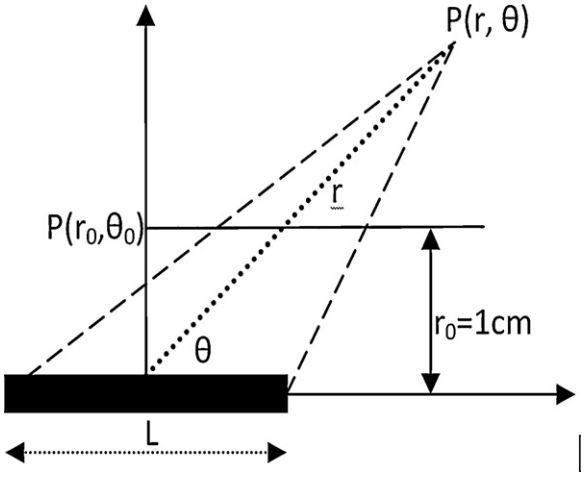


**Fig. 1 – Illustration of geometry assumed in the dose calculation formalism. Angle $\beta$ is that subtended by the active length at point P. The reference point is represented by P($r_0$, $\theta_0$).[5]**

### 1.1. *General formalism for two-dimensional case*

We restrict consideration to cylindrically symmetric sources, such as that illustrated in Fig. 1. For such sources, the dose distribution is two-dimensional and can be described in terms of a polar coordinate system with its origin at the source center where r is the distance to the point of interest and $\theta$ is the angle with respect to the long axis of the source (Fig. 1).

$P(r_0, \theta_0)$ is named a reference point. At this point it assumed that factors – except radial effects – that affect the dose rate are negligible. At any point the dose rate is given by

$$\dot{D}(r,\theta) = S_k \Lambda \frac{G(r,\theta)}{G(r_0,\theta_0)} g(r) F(r,\theta)$$

where $S_k$ is air-kerma strength, $\Lambda$ dose rate constant, and $G(r, \theta)$ geometry function that is completely mathematical formalism dependent on source dimensions. The radial dose function, $g(r)$, accounts for the effects of absorption and scatter in the medium along the transverse axis of the source. It is defined as:

$$g(r) = \frac{\dot{D}(r,\pi/2)G(1,\pi/2)}{\dot{D}(1,\pi/2)G(r,\pi/2)}$$

The anisotropy function accounts for the anisotropy of dose distribution around the source, including the effects of absorption and scatter in the medium. It is defined as:

$$F(r,\theta) = \frac{\dot{D}(r,\theta)G(r,\pi/2)}{\dot{D}(r,\pi/2)G(r,\theta)}$$

### 1.2. *Radioactive source–seed*

$^{125}$I is produced when $^{124}$Xe absorbs a neutron, and then decays via electron capture. $^{125}$I itself decays with a half life of 59.4 days, by electron capture to the first excited state of $^{125}$Te, which undergoes internal conversion 93% of the time and otherwise emits a 35.5 keV gamma ray. The electron capture and internal conversion processes give rise to characteristic X-rays.[5]

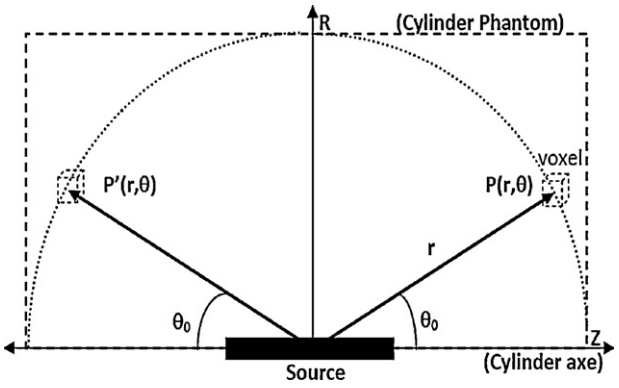


**Fig. 2 – Source symmetry on polar (R, Z) system: $P(r, \theta) = P'(r, \theta)$, where P is dose calculation point in the designed voxel.**

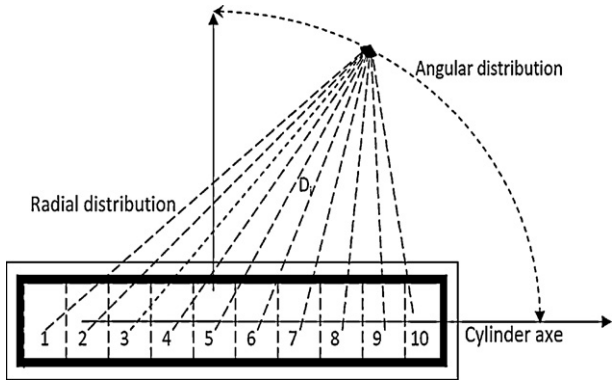


**Fig. 4 – Divisions of radioactive material of the seed on a cylindrical profile.**

### 1.3. *Simulation design: for source*

Using EGSnrc-MP code, it is possible to design cylindrical geometries and virtual objects. In the code, the phantom and the seed were designed as coaxial (equal axis) in cylindrical coordinate system. To limit cylinders, planar slabs were used. By using slabs and rings, voxels were performed in water phantom. These small volumes include dose calculation points. Voxels were selected as small as. Simulation was performed in 0–90° angular region of analytic system since the seed 6711 is symmetrical between 0° and 180° to vertical axle. It is assumed that all dose points of 0–90° region are equal to 90–180° region's points (Fig. 2).

### 1.4. *Radioactive seed geometry and physical properties*

Accurate knowledge of internal source geometry and construction details is especially important for Monte Carlo modeling (Fig. 3).

Radioactive material with 0.3 cm length was divided into 10 geometric pieces with 0.03 cm length. On the source axe, division lines were located at [−0.15, −0.12], [−0.12, −0.09], [−0.09, −0.06], [0.06, −0.03], [−0.03, 0], [0,0.03], [0.03, 0.06], [0.06, 0.09], [0.09, 0.12], [0.12, 0.15] lengths on the [−0.15, 0.15] length (Fig. 4).

This division process (Fig. 5) provides a similarity between seeds with multi-radioactive source and simple seeds like Model 6711 (Fig. 6a) and Theragenics200 palladium (Fig. 6b). Example source Theragenics has two radioactive sources in its capsule (Fig. 6b). Calculations relate to Theragenic source are made by using differential doses of two separate sources.

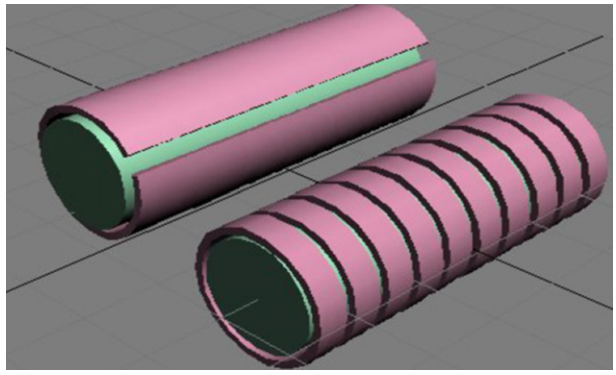

**Fig. 5 – Three-dimensional illustration of the seed-source geometry.**

### 1.5. *Phantom and voxel modeling*

Phantom where dose is calculated was modeled as a cylinder that coated the seed. Geometry is designed in association with the seed and source because planes cut all cylinders of source and phantom together. Modeling was performed as a source-phantom system. Voxels (this term is used in dosimetric area meaning a small volume of phantom and derived from a two-dimensional pixel term for three dimensions), which include analytic point of calculation, were located around the seed on polar coordinates. Instead of a cubic voxel, equivalent rings were used (Fig. 7) because of their cylindrical symmetry to decrease uncertainty of dose. It means that bigger volumes were acquired for every voxel. Intersections of vertical and horizontal lines produce cubic intersections (Fig. 8). Ring intersections go through these sections (Table 1).

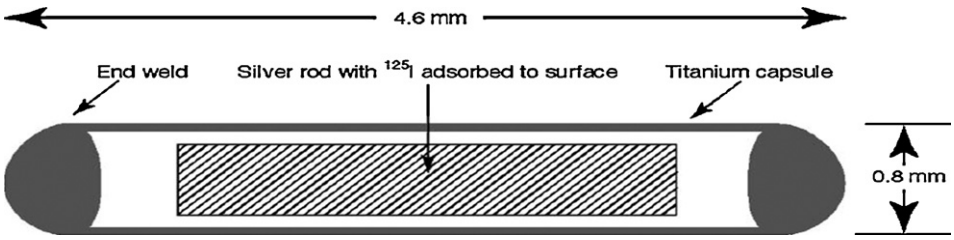


**Fig. 3 – Physical dimensions of Amersham Model 6711 $^{125}$I source.[5]**

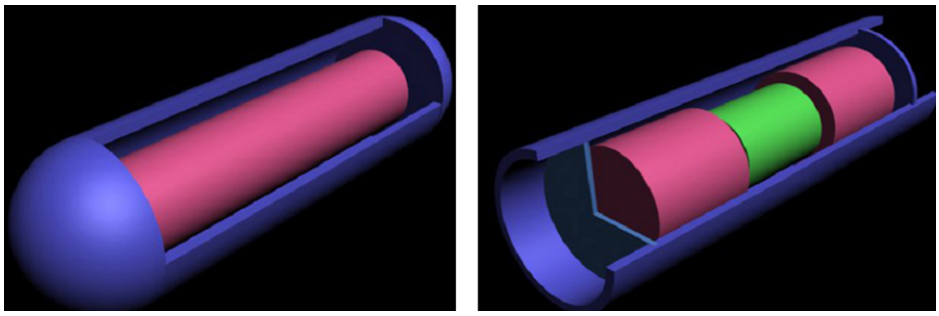

**Fig. 6 – (a and b) Intersections of Model 6711 and palladium Theragenic200 seeds.**

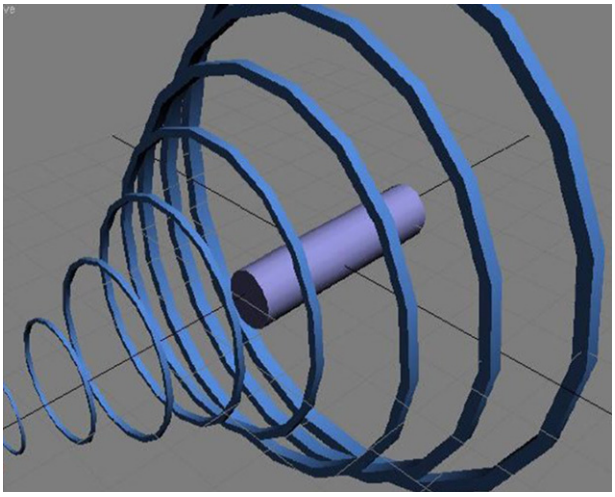

**Fig. 7 – Equivalent rings of voxels on polar points.**

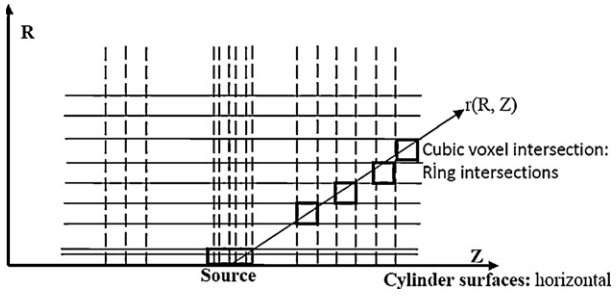


**Fig. 8 – This schema represents rings and slabs. Rings and slabs are produced from intersection of planes and cylinder shells. Intersections of vertical and horizontal lines produce cubic sections.**

**Table 1 – $^{125}$I decay spectrum (NNDC).**

| Decay | y(i) (Bq-s)$^{-1}$ | Photon energy (MeV) |
|---|---|---|
| γ1 | $6.68 \times 10^{-02}$ | $3.549 \times 10^{-02}$ |
| ce-K, γ1 | $8.02 \times 10^{-01}$ | $3.678 \times 10^{-03}$ |
| ce-L, γ1 | $1.08 \times 10^{-01}$ | $3.055 \times 10^{-02}$ |
| ce-M, γ1 | $2.15 \times 10^{-02}$ | $3.449 \times 10^{-02}$ |
| Kα1 X-ray | $7.44 \times 10^{-01}$ | $2.747 \times 10^{-02}$ |
| Kα2 X-ray | $4.00 \times 10^{-01}$ | $2.720 \times 10^{-02}$ |
| Kβ X-ray | $2.59 \times 10^{-01}$ | $3.100 \times 10^{-02}$ |
| L X-ray | $1.49 \times 10^{-01}$ | $3.770 \times 10^{-03}$ |
| Auger-K | $2.00 \times 10^{-01}$ | $2.270 \times 10^{-02}$ |

## 2. Mathematical approach

This work also offers a mathematical deduction for anisotropy function upon divided dose calculations. Differential doses can be added as:

$$\dot{D}(r,\theta) = \sum_i \dot{D}_i(r,\theta)$$

Anisotropy function is formed:

$$F(r,\theta) = \frac{\dot{D}(r,\theta)G(r,\pi/2)}{\dot{D}(r,\pi/2)G(r,\theta)} \rightarrow F(r,\theta) = \frac{\sum_i \dot{D}_i(r,\theta)}{\sum \dot{D}_i(r,\pi/2)} \times \frac{G(r,\pi/2)}{G(r,\theta)}$$

**Table 2 – For $r = 2$ cm $D(2, \theta)/D(2, \pi/2)$ of divisions.**

| $\theta$ | Div | | | | | | | | | |
|---|---|---|---|---|---|---|---|---|---|---|
| | 1 | 2 | 3 | 4 | 5 | 6 | 7 | 8 | 9 | 10 |
| 10 | **0.42** | **0.42** | **0.42** | 0.43 | 0.44 | 0.46 | 0.48 | 0.50 | 0.51 | 0.62 |
| 20 | **0.58** | **0.59** | **0.58** | 0.61 | 0.63 | 0.65 | 0.67 | 0.70 | 0.72 | 0.84 |
| 30 | **0.68** | **0.69** | **0.68** | 0.71 | 0.73 | 0.75 | 0.78 | 0.80 | 0.83 | 0.95 |
| 40 | **0.75** | **0.77** | **0.76** | 0.78 | 0.81 | 0.83 | 0.86 | 0.89 | 0.90 | 1.04 |
| 50 | **0.83** | **0.84** | **0.83** | 0.86 | 0.88 | 0.89 | 0.92 | 0.94 | 0.97 | 1.08 |
| 60 | **0.89** | **0.89** | **0.88** | 0.90 | 0.91 | 0.93 | 0.95 | 0.96 | 0.98 | 1.06 |
| 70 | **0.96** | **0.96** | **0.94** | 0.95 | 0.96 | 0.97 | 0.98 | 0.99 | 1.00 | 1.05 |
| 80 | **0.98** | **0.98** | **0.95** | 0.96 | 0.96 | 0.96 | 0.96 | 0.97 | 0.97 | 0.99 |

**Table 3 – For $r = 3$ cm $D(3, \theta)/D(3, \pi/2)$ of divisions.**

| $\theta$ | Div | | | | | | | | | |
|---|---|---|---|---|---|---|---|---|---|---|
| | 1 | 2 | 3 | 4 | 5 | 6 | 7 | 8 | 9 | 10 |
| 10 | **0.47** | **0.48** | **0.47** | 0.49 | 0.5 | 0.51 | 0.51 | 0.52 | 0.53 | 0.63 |
| 20 | **0.62** | **0.62** | **0.62** | 0.63 | 0.64 | 0.66 | 0.67 | 0.68 | 0.7 | 0.81 |
| 30 | **0.76** | **0.76** | **0.76** | 0.78 | 0.79 | 0.8 | 0.82 | 0.83 | 0.86 | 0.97 |
| 40 | **0.83** | **0.83** | **0.83** | 0.84 | 0.86 | 0.87 | 0.89 | 0.9 | 0.92 | 1.04 |
| 50 | **0.88** | **0.88** | **0.89** | 0.89 | 0.91 | 0.92 | 0.93 | 0.94 | 0.96 | 1.07 |
| 60 | **0.93** | **0.93** | **0.93** | 0.94 | 0.94 | 0.95 | 0.96 | 0.97 | 0.98 | 1.07 |
| 70 | **0.93** | **0.92** | **0.91** | 0.92 | 0.92 | 0.92 | 0.93 | 0.93 | 0.94 | 0.99 |
| 80 | **0.95** | **0.93** | **0.92** | 0.92 | 0.92 | 0.92 | 0.92 | 0.91 | 0.92 | 0.94 |

**Table 4 – For $r = 4$ cm $D(4, \theta)/D(4, \pi/2)$ of divisions.**

| $\theta$ | Div | | | | | | | | | |
|---|---|---|---|---|---|---|---|---|---|---|
| | 1 | 2 | 3 | 4 | 5 | 6 | 7 | 8 | 9 | 10 |
| 10 | **0.56** | **0.57** | **0.57** | **0.57** | **0.58** | **0.58** | 0.59 | 0.6 | 0.61 | 0.71 |
| 20 | **0.75** | **0.76** | **0.75** | **0.76** | **0.78** | **0.79** | 0.8 | 0.81 | 0.83 | 0.94 |
| 30 | **0.82** | **0.83** | **0.82** | **0.84** | **0.84** | **0.84** | 0.85 | 0.86 | 0.88 | 0.98 |
| 40 | **0.88** | **0.89** | **0.89** | **0.89** | **0.9** | **0.9** | 0.91 | 0.93 | 0.95 | 1.05 |
| 50 | **0.94** | **0.95** | **0.94** | **0.95** | **0.96** | **0.96** | 0.96 | 0.98 | 0.99 | 1.08 |
| 60 | **0.96** | **0.97** | **0.96** | **0.96** | **0.96** | **0.95** | 0.96 | 0.97 | 0.98 | 1.3 |
| 70 | **1.02** | **1.02** | **1.01** | **1.01** | **1.01** | **1** | 1 | 1.01 | 1.02 | 1 |
| 80 | **0.99** | **0.99** | **0.97** | **0.97** | **0.97** | **0.96** | 0.95 | 0.96 | 0.96 | 1.37 |

**Table 5 – For $r = 5$ cm $D(5, \theta)/D(5, \pi/2)$ of divisions.**

| $\theta$ | Div | | | | | | | | | |
|---|---|---|---|---|---|---|---|---|---|---|
| | 1 | 2 | 3 | 4 | 5 | 6 | 7 | 8 | 9 | 10 |
| 10 | 0.59 | 0.59 | 0.6 | 0.61 | 0.61 | 0.62 | 0.63 | 0.76 | 0.76 | 0.75 |
| 20 | **0.69** | **0.69** | 0.71 | 0.72 | 0.73 | 0.74 | 0.76 | 0.77 | 0.78 | 0.86 |
| 30 | **0.77** | **0.77** | 0.79 | 0.8 | 0.81 | 0.82 | 0.83 | 0.84 | 0.85 | 0.92 |
| 40 | **0.83** | **0.84** | 0.86 | 0.86 | 0.88 | 0.89 | 0.89 | 0.9 | 0.91 | 0.98 |
| 50 | **0.89** | **0.89** | 0.9 | 0.91 | 0.92 | 0.93 | 0.94 | 0.95 | 0.96 | 1.02 |
| 60 | **0.93** | **0.93** | 0.95 | 0.95 | 0.96 | 0.97 | 0.97 | 0.97 | 0.98 | 1.03 |
| 70 | **0.97** | **0.96** | 0.98 | 0.97 | 0.98 | 0.98 | 0.98 | 0.98 | 0.99 | 1.01 |
| 80 | **1** | **0.99** | 1 | 0.99 | 1 | 1 | 1 | 1 | 1 | 1 |

### 2.1. *Differential function definitions*

These definitions are offered by this study

$$F_i(r, \theta) = \frac{\dot{D}(r, \theta)}{\sum_i \dot{D}_i(r, \pi/2)}$$

Total anisotropy function can be written as:

$$F(r, \theta) = \sum_i F_i(r, \theta) \times \frac{G(r, \pi/2)}{G(r, \theta)}$$

where the "i" index is a representation of a segment number of the radioactive source. It was seen from calculation results (Tables 2–5) that for every $\theta$ angle in the same radial value, the fractions corresponding to the divisions were approximately equal to each other for distant divisions to calculation point. This specification can be shown. Bold values in the tables provide constant approach.

$$\frac{\dot{D}_1(r_n, \theta_m)}{\dot{D}_1(r_n, \pi/2)} = \frac{\dot{D}_2(r_n, \theta_m)}{\dot{D}_2(r_n, \pi/2)} = \frac{\dot{D}_3(r_n, \theta_m)}{\dot{D}_3(r_n, \pi/2)} = \cdots = \frac{\dot{D}_N(r_n, \theta_m)}{\dot{D}_N(r_n, \pi/2)} = C$$

where $m = 10^\circ, 20^\circ, 30^\circ, \ldots, 90^\circ$, $n$ is a distance index of dose calculation point to the source in cm unit and $C$ is constant.

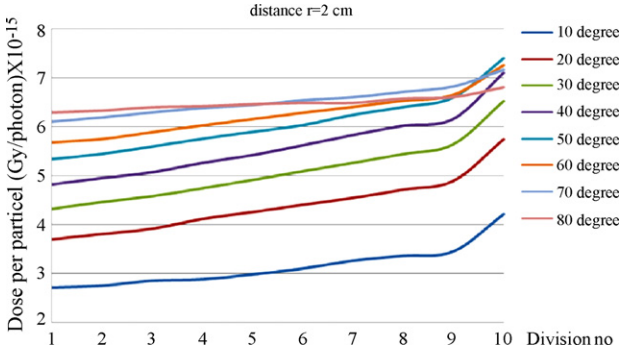


**Fig. 9 – For 2 cm radial values, angular dose distributions of virtual source divisions.**

## 3. Conclusion

For 2, 3, 4 and 5 cm radial values, angular dose distributions of virtual source divisions were determined (Figs. 9–12).

To shape aimed profile of dose multi-sources and maker are designed for such seeds (Fig. 6b). In this study firstly it

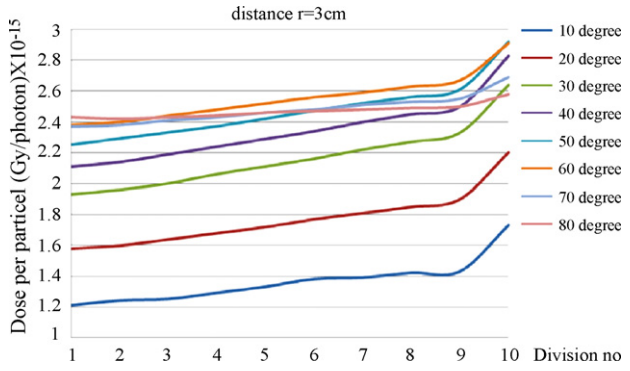


**Fig. 10 – For 3 cm radial values, angular dose distributions of virtual source divisions.**

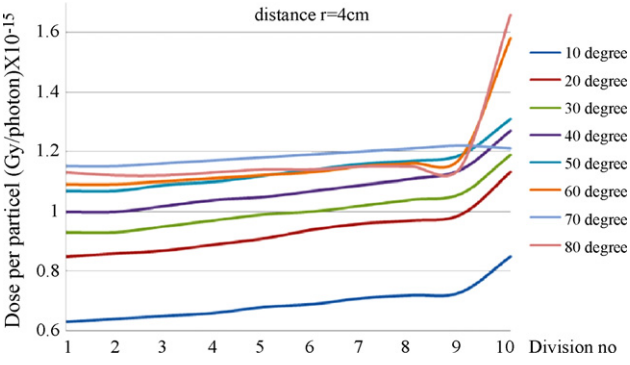


**Fig. 11 – For 4 cm radial values, angular dose distributions of virtual source divisions.**

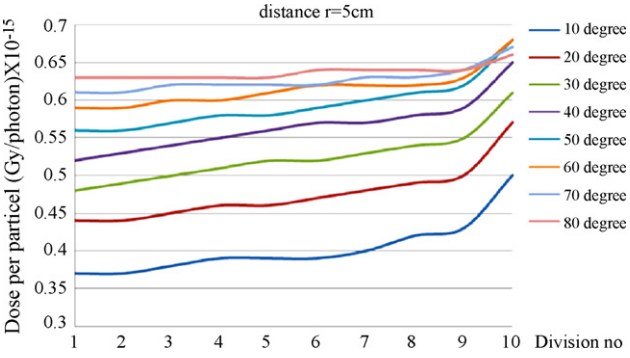


**Fig. 12 – For 5 cm radial values, angular dose distributions of virtual source divisions.**

is aimed that investigation novel designation approaches to acquire uniform dose profile along seed cylinder in tissue.

Constant value that is suggested in mathematical representation of anisotropy function is completely dependent on source specifications (geometry). C constant deduction cannot be seen clearly for distance longer than 3 cm (Table 2). Doses decrease rapidly beyond 1 cm for low energies of x photons of $^{125}$I so statistical errors increase. This situation causes non sensitive dose calculation.

Dose distributions of divisions are parallels until 10th division (Figs. 9–12) for different angles in several radial distances (2, 3, 4 and 5 cm). Ends of the source are more effective on distributions. It means that the most important contribution is made by the end regions of source cylinder. This must be taken into account in source designs.

## REFERENCES

1. Faiz MK. *The physics of radiation therapy*. 1st ed. USA: Lippincott Williams & Wilkins; 1984.
2. Hilaris BS, Nori D, Anderson LL. *Atlas of brachytherapy*. New York: MacMillan Publishing Co.; 1988.
3. Yu Y, Anderson LL, Li Z, Mellenberg DE, Nath R, Schell MC, et al. Permanent prostate seed implant brachytherapy: report of the American Association of Physicists in Medicine Task Group report no. 64. *Med Phys* 1999;**26**:2054–76.
4. Mettlin CJ, Murphy GP, Rosenthal DS, Menck HR. The national cancer data base report on prostate carcinoma after the peak in incidence rates in the U.S. *Cancer* 1998;**83**:1679–84.
5. Rivard MJ, Coursey M, Larry A, Hanson WF. Update of AAPM Task Group no. 43 report: A revised AAPM protocol for brachytherapy dose calculations. *Med Phys* 2004;**31**:663–74.
6. Nath R, Yue N. Dosimetric characterization of a newly designed encapsulated interstitial brachytherapy source of iodine-125 – model LS-1 Brachyseed. *Appl Rad Isot* 2002;**55**:813–21.
7. Mainegra E, Capote R, Lopez E. Radial dose function for $^{103}$Pd, $^{125}$I, $^{169}$Yb and $^{192}$Ir brachytherapy sources. *Phys Med Biol* 2000;**45**:703–17.
8. Williamson JF. Dosimetric characteristics of the DraxImage Model LS-1 I-125 interstitial brachytherapy source design: a Monte Carlo investigation. *Med Phys* 2002;**29**: 509–21.
9. Naseri A, Mesbahi A. Application of Monte Carlo calculations for validation of a treatment planning system in high dose rate brachytherapy. *Rep Pract Oncol Radiother* 2009;**4**: 200–4.
10. Johnson M, Colonias A, Parda D, Trombetta M, Gayou O, Reitz B, et al. Dosimetric and technical aspects of intraoperative I-125 brachytherapy for stage I non-small cell lung cancer. *Phys Med Biol* 2007;**52**:1237–2145.
11. Monge MR, Nag S, Nieroda C, Martin EW. Iodine-125 brachytherapy in the treatment of colorectal adenocarcinoma metastatic to the lever. *Cancer* 1999;**85**(6):1218–25.